

Phase relations in Fe–Ni–C system at high pressures and temperatures

O. Narygina · L. S. Dubrovinsky · N. Miyajima ·
C. A. McCammon · I. Yu. Kantor · M. Mezouar ·
V. B. Prakapenka · N. A. Dubrovinskaia · V. Dmitriev

Received: 19 May 2010 / Accepted: 10 August 2010 / Published online: 24 August 2010
© Springer-Verlag 2010

Abstract We performed comparative study of phase relations in $\text{Fe}_{1-x}\text{Ni}_x$ ($0.10 \leq x \leq 0.22$ atomic fraction) and $\text{Fe}_{0.90}\text{Ni}_{0.10-x}\text{C}_x$ ($0.1 \leq x \leq 0.5$ atomic fraction) systems at pressures to 45 GPa and temperatures to 2,600 K using laser-heated diamond anvil cell and large-volume press (LVP) techniques. We show that laser heating of Fe,Ni alloys in DAC even to relatively low temperatures can lead to the contamination of the sample with the carbon coming from diamond anvils, which results in the decomposition of the alloy into iron- and nickel-rich phases. Based on the results of LVP experiments with Fe–Ni–C

system (at pressures up to 20 GPa and temperatures to 2,300 K) we demonstrate decrease of carbon solubility in Fe,Ni alloy with pressure.

Keywords LH-DAC · Large-volume press · Martensitic transformation · Carbon solubility in Fe,Ni alloy

Introduction

Knowledge on the properties of the Earth's core (its structure and composition, temperature profile, etc.) as well as understanding of the processes driving its dynamics is essential for reliable modeling of the deep Earth's interior. Due to its inaccessibility the only insight into the properties of the Earth's core is provided by seismic observations (Ringwood 1979). The seismic data along with estimates of the bulk silicate Earth composition (Ringwood 1979; Allégre et al. 1995; O'Neill and Palme 1998; McDonough and Sun 1995) and meteoritic records provide some insights into the possible structure and composition of the Earth's core. It is now well established that the core consists of the liquid outer and solid inner parts, which are mainly composed by $\text{Fe}_{1-x}\text{Ni}_x$ alloy ($0.05 \leq x \leq 0.20$) with a small amount of light element(s) such as Si, S, O, H, C, etc., required to fulfill the density deficit, which accounts for ~6–10% difference between the outer core and liquid Fe, and 1–2% between the inner core and crystalline Fe (Birch 1952; Poirier 1994; McDonough and Sun 1995; Allégre et al. 1995).

Phase diagram of iron—the most abundant element in the core—has been extensively studied using both experimental and numerical approaches. Although melting curve of iron at high pressures is controversial (~2,000 K misfit between shockwave (Yoo et al. 1993; Brown and McQueen

Electronic supplementary material The online version of this article (doi:10.1007/s00269-010-0396-x) contains supplementary material, which is available to authorized users.

O. Narygina (✉) · L. S. Dubrovinsky · N. Miyajima ·
C. A. McCammon · I. Yu. Kantor · N. A. Dubrovinskaia
Bayerisches Geoinstitut, Universität Bayreuth,
95440 Bayreuth, Germany
e-mail: Olga.Narygina@ed.ac.uk

I. Yu. Kantor · M. Mezouar · V. Dmitriev
European Synchrotron Radiation Facility,
BP 220, 38043 Grenoble Cedex, France

V. B. Prakapenka
Center for Advanced Radiation Sources,
University of Chicago, Chicago, IL 60637, USA

Present Address:

O. Narygina
SUPA, School of Physics and Centre for Science at Extreme
Conditions, The University of Edinburgh, James Maxwell Clerk
Building, Mayfield Road, Edinburgh EH9 3JZ, UK

Present Address:

N. A. Dubrovinskaia
Institut für Geowissenschaften, Universität Heidelberg,
69120 Heidelberg, Germany

1986) and diamond anvil cell (Williams et al. 1987; Boehler 1993; Schen et al. 1998) experiments, with theoretical predictions laying in between (Laio et al. 2000; Alfè 2009) both experimental and theoretical approaches agree that at the Earth's core conditions the stable phase of pure solid iron most likely would be hexagonal closed packed (*hcp*) ϵ -phase (Akimoto 1987; Boehler 1986; Mao et al. 1987; Manghnani and Syono 1987; Dubrovinsky et al. 1998; Schen et al. 1998; Funamori et al. 1996; Dewaele et al. 2006; Vocadlo et al. 2000). However, the alloying effect of nickel and light element(s) also has to be taken into account. Even small amount of nickel, alloyed with iron, significantly enhances stability area of γ -phase to lower temperatures and to higher pressures (Huang et al. 1988, 1992; Lin et al. 2002; Mao et al. 2006; Dubrovinsky et al. 2007). The effect of the potential light core's components on the phase diagram of iron at high pressures and temperatures also has been extensively studied (Badding et al. 1991; Wood 1993; Fei and Mao 1994; Knittel and Williams 1995; Sanloup et al. 2000; Fei et al. 1995, 2000; Scott et al. 2001; Lin et al. 2002). However, the question regarding the composition and structural phase of the Earth's core remains unsolved mainly due to the lack of experiments under the relevant pressures and temperatures, which has led to inevitable extrapolations of experimental data to the Earth's core conditions.

Pressures and temperatures comparable with that in the core can be achieved in diamond anvil cells with in situ laser heating (LH-DAC) (Boehler 1993; Murakami et al. 2005; Mao et al. 2006; Dubrovinsky et al. 2007; Ohta et al. 2008; etc), which, however, may suffer from possible substantial pressure and temperature gradients, occurrence of chemical reactions, migration of the matter under study, etc. (Heinz et al. 1991; Prakapenka et al. 2003–2004; Fialin et al. 2009). The large-volume press (LVP) technique, on the other hand, provides more controllable experimental conditions due to the larger size of a pressure chamber, though the upper pressure limit is 28 GPa (in multianvil experiments with tungsten carbide anvils (Kubo and Akaogi 2000), which is less than that of the Earth's core. Combining both LH-DAC and LVP experiments we performed comparative study of the phase relations in $\text{Fe}_{1-x}\text{Ni}_x$ ($0.10 \leq x \leq 0.22$) to 45 GPa and 2,600 K and investigated the effect of carbon on the system at high pressures and temperatures.

Experimental procedure

The $\text{Fe}_{0.9}\text{Ni}_{0.1}$, $\text{Fe}_{0.85}\text{Ni}_{0.15}$ and $\text{Fe}_{0.78}\text{Ni}_{0.22}$ alloys used for LH-DAC and part of LVP experiments were synthesized from metallic rods by melting of appropriate amounts of iron (99.999% purity) and nickel (99.999% purity) in an

arc furnace in pure argon atmosphere. The samples were homogenized in vacuum at 900°C for 150 h. Their chemical and phase homogeneity were confirmed by electron-microprobe analyses and X-ray powder diffraction. Further details of synthesis and sample characterization were given in Dubrovinsky et al. (2001). A series of LVP runs were performed with the powder mixtures $\text{Fe}_{0.90}\text{Ni}_{0.10-x}\text{C}_x$ (where $0.01 \leq x \leq 0.04$ atomic fraction). The powders were thoroughly ground together under alcohol in order to obtain homogenized mixture, which then was dried and placed into a capsule. Two types of capsule were used: (1) “simple” cylindrical capsule made of MgO compressed powder; and (2) “composite” capsule, containing a single crystal of NaCl placed inside the MgO capsule. NaCl was used in order to eliminate oxygen from the system.

For LH-DAC experiments the modified Merrill–Basset DAC equipped with diamond anvils of 250 and 300 μm culet size was used. The 10–15- μm -thick foils of synthetic $^{57}\text{Fe}_{0.9}\text{Ni}_{0.1}$ and $^{57}\text{Fe}_{0.78}\text{Ni}_{0.22}$ alloys, sandwiched between two 10- μm -thick pellets of LiF or NaCl, along with few ruby chips (for pressure calibration according to ruby fluorescence scale by Mao et al. (1986)) were loaded into a 100- to 125- μm hole drilled in Re gasket pre-indented to 30–35 μm . LiF and NaCl were used as a pressure transmitting medium, thermal insulation from diamond anvils as well as an internal X-ray diffraction (XRD) pressure marker. We used LiF and NaCl equation of states from Liu et al. (2007) and Brown (2000), respectively). LiF and NaCl (both powder and single crystals, used for the LVP and DAC runs) were dried before use at 200°C for 12 h to eliminate water.

The high-resolution angle dispersive XRD experiments with ex situ laser heating were performed at (1) high-brilliance X-ray diffractometer at the Bayerisches Geoinstitut, Bayreuth, Germany, with 0.7108 Å wavelength radiation and the beam size on the sample of 30 μm^2 , (2) Swiss–Norwegian beamline at the European Synchrotron Radiation Facility (ESRF), Grenoble, France, with 0.7002 Å radiation wavelength and the beam size on the sample of 40 μm^2 , and (3) at beamline ID27 (ESRF) with 0.3738 Å wavelength radiation and the beam size on the sample of approximately 10 μm^2 . The high-resolution XRD experiments with in situ double-side Nd:YLF laser heating system were carried out at GSECARS beamline, Sector 13 of the Applied Photon Source, Chicago, USA. The size of the laser beam varied from 20 to 30 μm in diameter with a temperature variation of ± 100 K within the beam at temperatures in the order of 3,000 K. Heating duration in different experiments was from 10 to 30 min. Temperature was measured using multiwavelength spectroradiometry. The radiation with 0.3344 Å wavelength and a CCD MAR detector were used. Two-dimensional XRD images we integrated azimuthally using Fit2D

software (Hammersley 1998). Rietveld refinement was performed with the GSAS package (Larson and Von Dreele 2004).

The quenched experiments at low pressures (0.5–3 GPa) were performed in the end-loaded piston-cylinder apparatus. For the high-pressure experiments (9–20 GPa) the 6–8 Kawai-type multianvil press were employed. For the piston-cylinder runs the half-inch talc-Pyrex glass assembly equipped with a graphite heater was used. Temperature was controlled by a $W_{75}Re_{25}/W_{97}Re_3$ thermocouple (type D). For multianvil experiments the 10/5 (octahedral edge length/tungsten-carbide anvil truncation in mm) assembly with $LaCrO_3$ heater was employed in the 1,200-ton press. The pressure calibration curve is based on that developed by Frost et al. (2001). Time of LVP runs varied from 4 to 14 h.

Samples recovered from both LH-DAC and LVP experiments were analysed by X-ray powder diffraction, Mössbauer spectroscopy (described in detail in McCammon et al. 1992), transmission electron microscopy (TEM) and scanning electron microscopy (SEM) using a Leo Gemini 1530 scanning electron microscope. For the microstructural analyses of the samples recovered from the LH-DAC experiments the upper layer of a gasket was carefully grained off in order to get exposure of the sample enclosed in a gasket hole and a 5-nm graphite coating layer was required to reduce charging. The capsules of the LVP runs were cut in half; one part was polished for SEM measurements (due to their high electrical conductivity these samples did not require any coating); a thin layer cut from the another part of a sample was used for Mössbauer

spectroscopy, XRD and TEM (the latter required additional thinning of a sample foil by Ar-milling method).

Conventional TEM imaging, selected area electron diffraction (SAED) and energy-dispersive X-ray spectroscopy (EDXS) were performed on a Philips CM20 FEG TEM operating at 200 kV. The Ni/Fe ratios of Fe,Ni–C alloys were calculated by the Cliff–Lorimer method (Cliff and Lorimer 1975) with a pre-installed k-factor (Ni/Fe) of 1.067 in NSS. 2.1 EDXS system (Thermo Scientific). Absorption correction was not performed because of the relatively thin areas for the analysis of characteristic Ni– $K_{\alpha,\beta}$ and Fe– $K_{\alpha,\beta}$ X-rays.

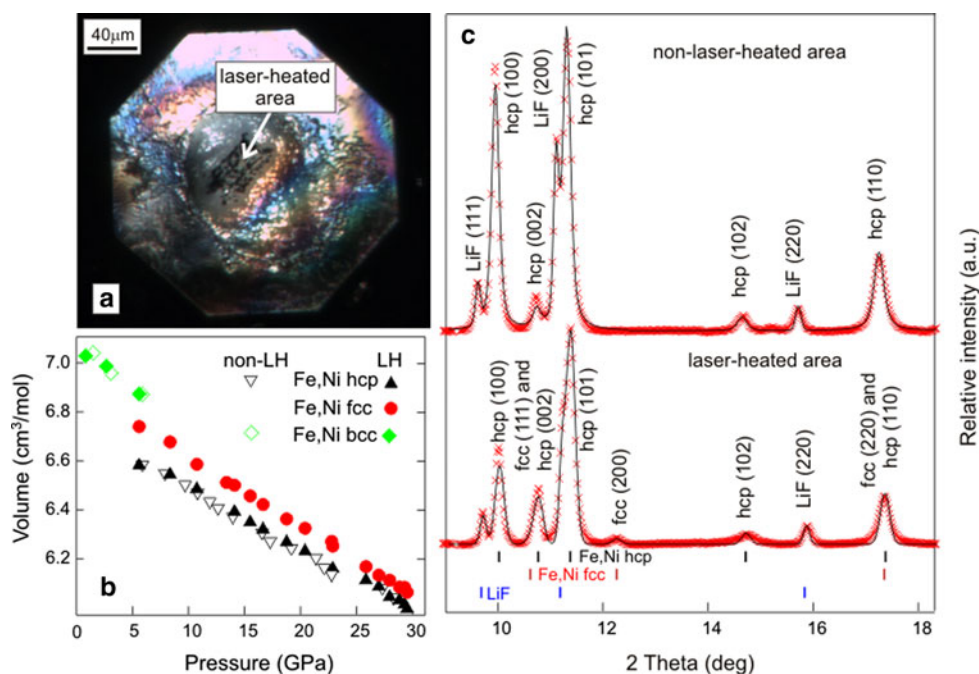
Experimental results

XRD study of Fe,Ni alloys, employing LH-DAC

$Fe_{0.9}Ni_{0.1}$ alloy at pressures to 30 GPa

The thin (15 μm) foil of $^{57}\text{Fe}_{0.90}\text{Ni}_{0.10}$ alloy, placed between two layers of LiF, was compressed in DAC to 30 (1) GPa; the XRD patterns taken from several areas of the sample at 30 GPa show presence of *hcp*-Fe,Ni alloy and LiF. The central part, $\sim 20 \mu\text{m} \times 40 \mu\text{m}$, was laser heated to 2,000 K (± 100 K) (see Fig. 1a). On the decompression from 30 GPa to the ambient pressure we collected XRD spectra from the heated and non-heated areas of the sample (this experiment was performed at ID27, ESRF). In the laser-heated spot we detected presence of *fcc*-structured phase along with *hcp*-Fe,Ni, while in the non-laser-heated

Fig. 1 **a** Photo-image of the $Fe_{0.90}Ni_{0.1}$ sample, central part of which was laser heated to 2,000 K at 30 GPa; **b** Molar volumes of *hcp*-, *fcc*- and *bcc*-structured Fe,Ni phases in heated (*solid symbols*) and non-heated (*open symbols*) areas of the sample; **c** XRD patterns ($\lambda = 0.3738 \text{ \AA}$) collected at 15.5 (0.1) GPa and room temperature from the heated and non-heated areas of the $Fe_{0.90}Ni_{0.1}$ sample



area only initial *hcp*-Fe,Ni alloy was found (see Fig. 1b, c). The presence of *fcc*-*hcp* phase assemblage in the heated area was tracked down from 30 to ~6 GPa, where both phases eventually transformed to their *bcc*-polymorphs. Since *fcc*-phase, detected in the heated area, accounts only for about 6 (1) wt%, it is impossible to extract XRD parameters of its *bcc*-structured polymorph, washed by the strong reflections coming from the predominant Fe,Ni *bcc*-phase. At the same pressure (~6 GPa) the *hcp*-*bcc* structural transition occurred in the non-heated area (Fig. 1b). Molar volumes of the *hcp*-Fe,Ni phase in the laser-heated area (closed triangles) and those in the non-heated part (open triangles) are identical within the uncertainty of measurements (Fig. 1b). The same is valid for the *bcc*-phases, formed below 6 GPa in both areas.

Coexistence of *hcp* and *fcc*-structured phases of Fe,Ni alloy at high pressure and temperature was previously observed in DAC experiments (Lin et al. 2002; Mao et al. 2006). Presence of *fcc*-Fe at room temperature was detected in multianvil (Kubo et al. 2003) and DAC experiments (Komabayashi et al. 2009) with pure Fe, which was explained by kinematical effects.

$Fe_{0.78}Ni_{0.22}$ at pressures to 52 GPa and temperatures to 2,600 K

Another in situ XRD experiment was carried out with $Fe_{0.78}Ni_{0.22}$ alloy at pressures to 44 (1) GPa and temperatures to 2,600 (50) K (GCECARS, Sector 13, APS). $Fe_{0.78}Ni_{0.22}$ sample was compressed to 22 (1) GPa; then, five series of laser-heating (from 10 to 30 min each), quenching and compression were performed (Fig. 2). First, second and third series of the high-temperature XRD data were collected during gradual decrease of temperature from 1,800–2,000 to 1,500–1,450 K, while fourth and fifth series of data were collected upon gradual increase of temperature. The sequence of measurements is shown in Fig. 2 by arrows.

Below 30 GPa, all XRD spectra collected (first and second laser-heating series) suggest presence of the single *fcc*-structured Fe,Ni phase along with LiF, used as the pressure-transmitting medium (Fig. 3, bottom). During third laser heating of the $Fe_{0.78}Ni_{0.22}$ we detected appearance of another *fcc*-structured phase at ~29.0(5) GPa and 2,000 (20) K (Fig. 3, in the centre). The difference in molar volume between the two *fcc*-phases is $0.05 (1) \text{ cm}^3 \text{ mol}^{-1}$ at 29.0 (5) GPa and 2,000 (20) K. Entire XRD data set, collected during third laser heating [30 (2) GPa and temperatures from 2,000 (20) to 1,450 (20) K], four XRD spectra, obtained at the beginning of the fourth laser heating [36 (1) GPa and temperatures from 1,450 (20) to 1,700 (20) K] as well as room temperature data collected in between suggest presence of two *fcc*-phases (closed circles

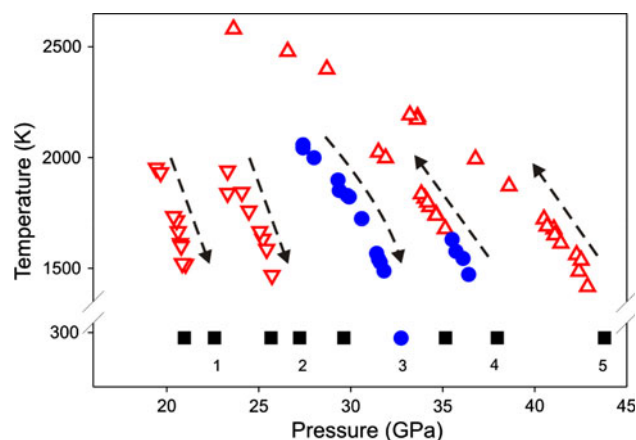


Fig. 2 Diagram presenting pressure and temperature conditions, achieved in five series of compression, laser heating and quenching of $Fe_{0.78}Ni_{0.22}$ alloy. Arrows show the sequence of the measurements. Red open triangles up and down correspond to data points collected during laser heating; room temperature points are shown by solid black squares. Different orientation of the red triangles distinguishes data points collected before (down) and after (up) the sequence of XRD spectra with “doubled” *fcc*-reflections (blue closed circles)

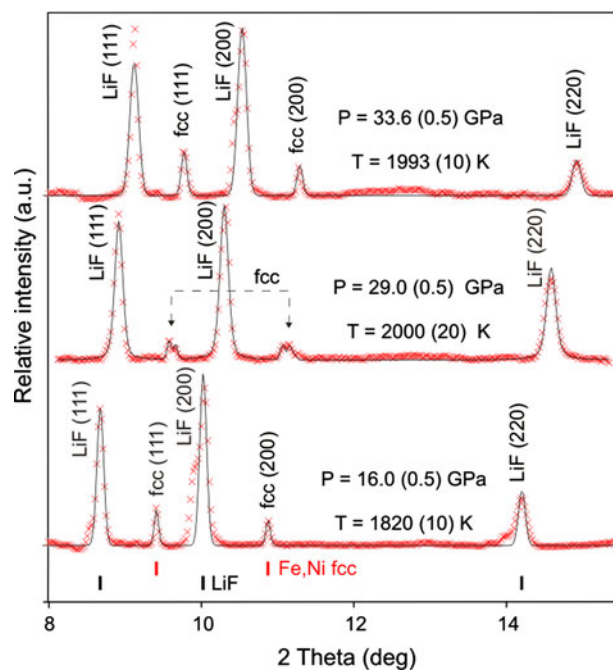


Fig. 3 XRD patterns ($\lambda = 0.3344 \text{ \AA}$) collected during in situ laser heating of the $Fe_{0.78}Ni_{0.22}$ sample in DAC. Red crosses correspond to experimental data, while black solid lines show Rietveld refinement of the data. “Doubling” of “*fcc*” peaks is highlighted by arrows. Broadening of LiF peaks on the bottom spectrum suggests presence of a certain thermal gradient during laser heating

in Fig. 2). At temperatures above 1,700 K and pressures over 35 GPa (high temperature part of the fourth and the entire fifth laser-heating series in Fig. 2), only *fcc*-phase with the higher volume was detected (see Figs. 2, 3, top spectrum).

An obvious explanation for the observed doubling of “*fcc*”-peaks is inhomogeneous heating. For example, the spectrum shown on the bottom in Fig. 3 with nice and narrow “*fcc*”-peaks indeed was collected from an area with high thermal gradient, which caused significant broadening of LiF-peaks. However, in the case of spectrum with two *fcc*-phases (Fig. 3, in the centre) LiF-peaks are rather narrow; consequently the thermal gradient, if it existed, must have been negligibly small and obviously cannot explain the 0.03 Å difference in lattice parameter between the two *fcc*-phases. Two other possible explanations are (1) iso-structural phase transition, occurring at high pressures and temperatures or (2) chemical reaction during laser heating, which will be discussed later.

Comparative study of $\text{Fe}_{1-x}\text{Ni}_x$ ($0.10 \leq x \leq 0.22$) at high pressures and temperatures by means of LH-DAC and LVP techniques

In another series of LH-DAC and LVP experiments, $\text{Fe}_{1-x}\text{Ni}_x$ ($0.10 \leq x \leq 0.22$) alloy samples were subjected to the same pressures and temperatures as in the aforementioned LH-DAC experiments (see Table 1). The recovered products were analysed by XRD, Mössbauer spectroscopy, SEM and TEM. For comparison the results of one of the paired LH-DAC and multianvil runs is shown in Fig. 4. In these two experiments $\text{Fe}_{0.90}\text{Ni}_{0.10}$ sample was heated to 2,000 (50) K at 20 (1) GPa and the duration of heating in both cases was about 5 min. XRD spectrum collected from the $\text{Fe}_{0.90}\text{Ni}_{0.1}$ recovered after laser-heating in DAC (Fig. 4c) shows weak reflections of *fcc*-Fe-bearing phase along with the reflections of the *bcc*-Fe,Ni phase, LiF (pressure-transmitting medium and thermal insulation) and rhenium gasket. Mössbauer spectrum collected from this sample also suggests presence of two iron-bearing phases (see Fig. 4a, on the top): (1) the magnetic component (light grey sextet) with the hyperfine parameters typical of *bcc*-Fe,Ni (central shift, CS, about 0.040 mm s⁻¹ relative to α -iron and hyperfine magnetic field, B, is 34.18 T) and (2) nonmagnetic or anti-ferromagnetic component (blue singlet with CS = -0.07 (0.01) mm s⁻¹), which was assigned to the *fcc*-Fe,Ni phase, known to be antiferromagnetic (Stixrude et al. 1994; Cohen and Mukherjee 2004; Shallcross et al. 2006). The observed value of the magnetic field of *bcc*-Fe,Ni alloy (34.2(2)) T is higher than that for pure α -iron (~33 T). The same effect on the internal magnetic field of iron has the alloying of Co (Greenwood and Gibb 1971), which was ascribed to the increased local exchange potential and the spin density. Note that *fcc*-Fe,Ni phase was found in all Fe,Ni alloy samples, recovered from the LH-DAC runs at pressures to 35 GPa (the maximum pressure achieved in this series of experiments) and temperatures to 2,300 K. By contrast, all Fe,Ni alloy samples, recovered after multianvil runs, performed at identical

pressures and temperatures, yielded single *bcc*-structured Fe,Ni phase with trace amount of (Fe,Ni)O as revealed by SEM (Fig. 4b, d, bottom).

Thus, summarizing the results, formation of the second *fcc*-structured Fe-bearing phase in addition to the predominant Fe,Ni alloy phase, which is stable at room temperature and even at room pressure in some experiments, was observed in all LH-DAC runs with $\text{Fe}_{1-x}\text{Ni}_x$ ($0.1 \leq x \leq 0.22$) alloys at 15–45 GPa and 1,450–2,600 K; Table 1, while quenched products of the LVP runs, performed with the same samples at the pressures and temperatures close to that in LH-DAC experiments (15–20 GPa and 1,800–2,200 K) revealed the presence of single *bcc*-structured Fe,Ni phase (Fig. 4b, d) (Table 1).

Discussion

$\text{Fe}_{1-x}\text{Ni}_x$ ($0.1 \leq x \leq 0.22$) alloys at pressures to 45 GPa and temperatures to 2,600 K: LH-DAC vs. multianvil experiments

The only plausible explanation for the observed discrepancy between results obtained with two different high-pressure techniques (Fig. 4) is the presence of contaminating material in LH-DAC experiments which reacts with the sample and leads to its decomposition. Careful preparation of a DAC experiment allows eliminating any possible contamination excluding carbon diffusing from diamond anvils that may react with a sample material during laser-heating as was previously shown by Prakapenka et al. 2003–2004 and Rouquette et al. (2008).

In order to check this hypothesis we simulated conditions of a DAC experiment in multianvil press, adding 1 wt% diamond powder (40–60 μm , 99.9% purity) into the capsule. Reaction of diamond powder with $\text{Fe}_{0.9}\text{Ni}_{0.1}$ alloy at 20 (1) GPa and 2,000 (50) K leads to the formation of carbon bearing *fcc*-structured Fe,Ni phase (blue singlet in Fig. 5) and *bcc*-Fe,Ni phase (light grey sextet in Fig. 5) and to the precipitation of Fe_3C carbide (dark grey sextet in Fig. 5). Comparing the result of the “DAC simulating” multianvil runs (Fig. 5) with that obtained in LH-DAC quench experiments (Fig. 4a, c) we conclude that the discrepancy between the results of the LH-DAC and multianvil quench experiments (Fig. 4) as well as the coexistence of *hcp*- and *fcc*-Fe,Ni phases and “doubling” of “*fcc*”-peaks observed in in situ XRD experiments with LH-DAC (Figs. 1, 3), is related to the contamination of Fe,Ni alloy by carbon. Specifically, upon laser heating to high temperatures (2,000–2,500 K) carbon from diamond anvils diffused through the thermal insulation layers of LiF (or NaCl or Ne) and eventually was incorporated by the *fcc*-Fe,Ni phase, which necessarily shifted the *fcc*-*bcc* phase boundary towards lower temperatures.

Table 1 Experimental conditions and resulting phase assemblages for LH-DAC and LVP runs with $\text{Fe}_{1-x}\text{Ni}_x$ and $\text{Fe}_{0.9}\text{Ni}_{1-x}\text{C}_x$ systems

Run	Starting material chemical composition	PTM	P (GPa)	T (K)	HP technique	Phases detected in the recovered samples
(Fe,Ni) alloys						
1	$\text{Fe}_{0.90}\text{Ni}_{0.10}$	Ne	15.6	1,700	DAC	bcc + fcc
2	$\text{Fe}_{0.90}\text{Ni}_{0.10}$	Ne	31.0	1,800	DAC	bcc + fcc
3	$\text{Fe}_{0.78}\text{Ni}_{0.22}$	LiF	25.0	1,600	DAC	bcc + fcc
4	$\text{Fe}_{0.90}\text{Ni}_{0.10}$	LiF	23.0	1,500	DAC	bcc + fcc
5	$\text{Fe}_{0.90}\text{Ni}_{0.10}$	LiF	20.0	2,000	DAC	bcc + fcc
6	$\text{Fe}_{0.90}\text{Ni}_{0.10}$	LiF	27.0	1,800	DAC	bcc + fcc
7	$\text{Fe}_{0.90}\text{Ni}_{0.10}$	–	10.0	2,000	LVP	bcc + (Fe,Ni)O
8	$\text{Fe}_{0.90}\text{Ni}_{0.10}$	–	15.0	2,200	LVP	bcc + (Fe,Ni)O
9	$\text{Fe}_{0.90}\text{Ni}_{0.10}$	–	15.0	1,800	LVP	bcc + (Fe,Ni)O
10	$\text{Fe}_{0.85}\text{Ni}_{0.15}$	–	17.0	1,900	LVP	bcc + (Fe,Ni)O
11	$\text{Fe}_{0.78}\text{Ni}_{0.22}$	–	20.0	2,100	LVP	bcc + (Fe,Ni)O
12	$\text{Fe}_{0.90}\text{Ni}_{0.10} + 1 \text{ wt\% C}$	–	20.0	2,100	LVP	bcc + fcc + (Fe,Ni)O + (Fe,Ni) ₃ C
(Fe,Ni,C) powder mixtures						
13	$\text{Fe}_{0.90}\text{Ni}_{0.09}\text{C}_{0.01}$	–	0.5	2,050	LVP	bcc + fcc + (Fe,Ni)O
14	$\text{Fe}_{0.90}\text{Ni}_{0.09}\text{C}_{0.01}$	–	1.0	2,050	LVP	bcc + fcc + (Fe,Ni)O
15	$\text{Fe}_{0.90}\text{Ni}_{0.09}\text{C}_{0.01}$	–	2.0	2,050	LVP	bcc + fcc + (Fe,Ni)O
16	$\text{Fe}_{0.90}\text{Ni}_{0.09}\text{C}_{0.01}$	–	2.5	2,050	LVP	bcc + fcc + (Fe,Ni)O
17	$\text{Fe}_{0.90}\text{Ni}_{0.09}\text{C}_{0.01}$	–	3.0	2,050	LVP	bcc + fcc + (Fe,Ni)O
18	$\text{Fe}_{0.90}\text{Ni}_{0.09}\text{C}_{0.01}$	–	9.0	2,010	LVP	bcc + fcc + (Fe,Ni)O
19	$\text{Fe}_{0.90}\text{Ni}_{0.09}\text{C}_{0.01}$	–	20.0	2,050	LVP	bcc + fcc + (Fe,Ni)O
20	$\text{Fe}_{0.90}\text{Ni}_{0.08}\text{C}_{0.02}$	–	1.0	2,050	LVP	bcc + fcc + (Fe,Ni)O
21	$\text{Fe}_{0.90}\text{Ni}_{0.08}\text{C}_{0.02}$	–	2.0	2,050	LVP	bcc + fcc + (Fe,Ni)O
22	$\text{Fe}_{0.90}\text{Ni}_{0.08}\text{C}_{0.02}$	–	3.0	2,050	LVP	bcc + fcc + (Fe,Ni)O
23	$\text{Fe}_{0.90}\text{Ni}_{0.08}\text{C}_{0.02}$	–	9.0	2,300	LVP	bcc + fcc + (Fe,Ni)O
24	$\text{Fe}_{0.90}\text{Ni}_{0.08}\text{C}_{0.02}$	–	20.0	2,400	LVP	bcc + fcc + (Fe,Ni)O
25	$\text{Fe}_{0.90}\text{Ni}_{0.07}\text{C}_{0.03}$	–	2.0	2,050	LVP	bcc + fcc + (Fe,Ni)O
26	$\text{Fe}_{0.90}\text{Ni}_{0.07}\text{C}_{0.03}$	–	2.0	2,050	LVP ^a	bcc + fcc
27	$\text{Fe}_{0.90}\text{Ni}_{0.07}\text{C}_{0.03}$	–	2.0	2,050	LVP ^{ab}	bcc + fcc
28	$\text{Fe}_{0.90}\text{Ni}_{0.07}\text{C}_{0.03}$	–	3.0	2,050	LVP	bcc + fcc + (Fe,Ni)O
29	$\text{Fe}_{0.90}\text{Ni}_{0.07}\text{C}_{0.03}$	–	9.0	2,300	LVP	bcc + fcc + (Fe,Ni)O
30	$\text{Fe}_{0.90}\text{Ni}_{0.07}\text{C}_{0.03}$	–	20.0	2,300	LVP	bcc + fcc + (Fe,Ni)O
31	$\text{Fe}_{0.90}\text{Ni}_{0.06}\text{C}_{0.04}$	–	3.0	2,050	LVP	bcc + fcc + (Fe,Ni)O
32	$\text{Fe}_{0.90}\text{Ni}_{0.06}\text{C}_{0.04}$	–	9.0	2,300	LVP	bcc + fcc + (Fe,Ni)O
33	$\text{Fe}_{0.90}\text{Ni}_{0.06}\text{C}_{0.04}$	–	20.0	2,300	LVP	bcc + fcc + (Fe,Ni) ₃ C + (Fe,Ni)O

Duration of heating in LH-DAC and LVP runs was about 5 min

PTM pressure transmitting medium

^a LVP runs with a “composite” capsule consisting of a single crystal of NaCl placed inside a MgO capsule

^b LVP runs with gradual cooling from 2,050 to 1,000 K, followed by rapid quenching to room temperature

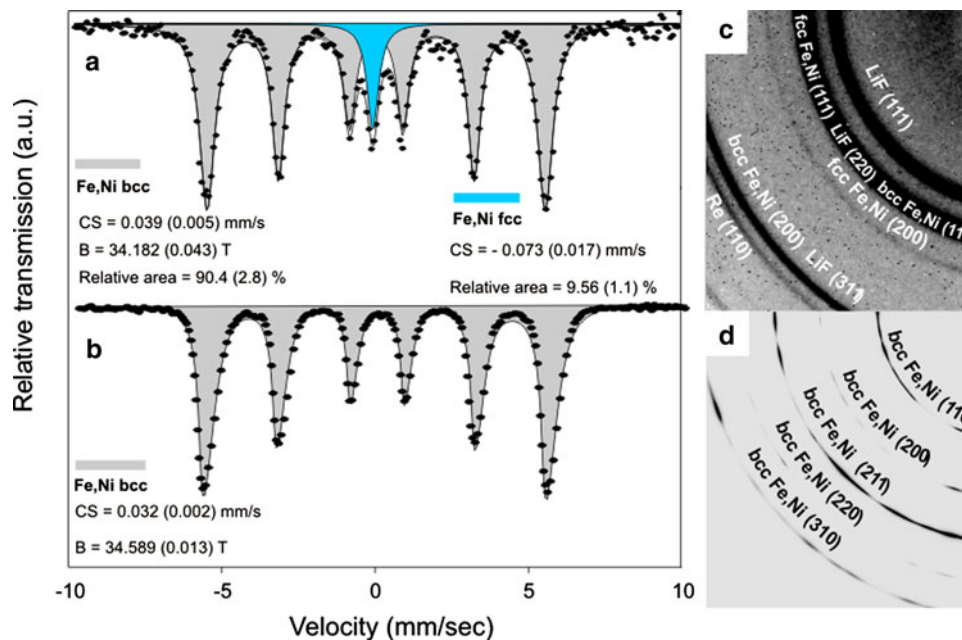
Effect of carbon on the phase relations in Fe,Ni system at elevated pressures and temperatures: martensitic transformation

According to the equilibrium Fe–C phase diagram at ambient pressure carbon solubility in *fcc*-structured phase of iron can be as high as 2.06 wt% at ~1,400 K while

bcc-iron can incorporate only about 0.0022 wt% carbon at ~1,000 K (Jiang and Carter 2003). Since atomic radius of carbon is almost twice smaller than that of iron in both *bcc* and *fcc*-structured iron phases, carbon atoms occupy tetrahedral or octahedral interstices (Fig. 6).

Pressure effect on the carbon solubility in Fe and Fe,Ni alloys is poorly constrained. Decrease of carbon solubility

Fig. 4 Mössbauer and XRD spectra collected at ambient conditions from Fe_{0.90}Ni_{0.10} alloy recovered after heating to 2,000 (50) K at 20 (1) GPa in LH-DAC (a, c) and in the multianvil (b, d)



in Fe or Fe,Ni alloys upon compression has been reported by Wood 1993, Huang et al. 2005 and Lord et al. 2009. However, this conclusion has been challenged by Fei et al. (2007), who observed an increase of carbon solubility in iron with the increase of pressure. Due to the significantly higher solubility of carbon in *fcc*-Fe in comparison with *bcc*-Fe, gradual cooling of C-bearing *fcc*-Fe to room temperature leads to formation of *bcc*-Fe and Fe₃C carbide. However in our LH-DAC and LVP experiments the rapid cooling of the *fcc*-structured Fe_{1-x}Ni_x alloys containing a certain amount of carbon results in the non-equilibrium diffusion less martensitic transformation (Martens 1878a, b, c). Martensite is a metastable supersaturated Fe–C solid solution with a body-centred tetragonal (*bct*) structure, slightly distorted form of *bcc* iron; the degree of distortion is linked to the carbon concentration (Kurdjumov and Kaminsky 1928, 1929; Mazur 1950; Roberts 1953; Xiao et al. 1995) and, based on the geometry of the lattice, can be estimated in the following way:

$$a = a_0 - \beta \cdot \rho_C, \quad c = a_0 + \alpha \cdot \rho_C, \quad c/a = 1 + \gamma \cdot \rho_C, \quad (1)$$

where a_0 is the lattice parameter of *bcc*-Fe, a and c are the lattice parameters of the Fe–C martensite, ρ_C is carbon content in wt%, $\alpha = 0.116$ (0.002), $\beta = 0.013$ (0.002) and $\gamma = 0.046$ (0.001). Martensitic transformation occurs over a certain temperature interval, defined by a martensitic start temperature, M_s , and a martensitic final temperature, M_f , at which the entire *fcc*-phase should have transformed into martensite. At any intermediate temperature ($M_f < T < M_s$) a certain amount of *fcc*-structured phase remains untransformed. Both the M_s and M_f temperatures of Fe–Ni–C system are significantly lowered by the alloying

of Ni or/and C (Stevens and Haynes 1956; Troiano and Greninger 1946; Shackelford 2001). Another factor which shifts the transformation towards lower temperatures is a pressure increase (Patel and Cohen 1953; Kakeshita et al. 1988; Xie et al. 1993). The effect of alloying on the M_f temperature can be estimated based on the empirical relation, developed by Stevens and Haynes (1956) and Gulyaev (1977) for low-carbon steels at ambient pressure:

$$M_f(\text{K}) = 639 - 17 \cdot \rho_{\text{Ni}} - 474 \cdot \rho_C, \quad (2)$$

where ρ_{Ni} and ρ_C are the weight percentages of Ni and C, respectively. Other investigators suggest that the alloying of Ni and C results in even greater decrease of the M_f (Shackelford 2001). Thus for Fe,Ni alloys, used in this work, the values of M_f temperature are predicted to decrease to 496 (15) K, 384 (15) K and 321 (15) K at 10, 15 and 22 wt% of Ni concentration, respectively. Addition of 0.2–0.3 wt% C would lower these values of M_f below the room temperature even at 0.5 GPa (Stevens and Haynes 1956; Troiano and Greninger 1946; Shackelford 2001; Patel and Cohen 1953; Kakeshita et al. 1988; Xie et al. 1993) the lowest pressure achieved in the present work. We suggest that the presence of the *fcc*-structured Fe,Ni phase at room temperature in the case of both LH-DAC experiments (Figs. 1, 4a, c) and “DAC-simulating” LVP runs (Fig. 5) can be explained by the incomplete martensitic transformation induced by the rapid temperature decrease.

Carbon solubility in Fe,Ni alloy at elevated pressures and temperatures

To define the maximum amount of carbon, which can dissolve in Fe,Ni alloy at elevated pressures and temperatures

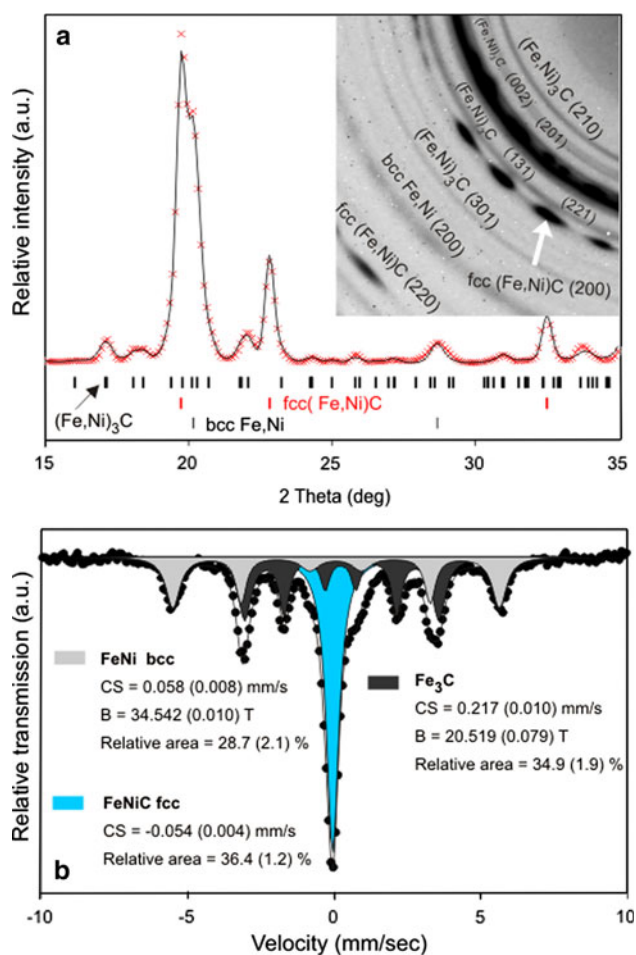


Fig. 5 XRD ($\lambda = 0.7108 \text{ \AA}$) (**a**) and Mössbauer spectrum (**b**) collected at ambient conditions from $\text{Fe}_{0.90}\text{Ni}_{0.10}$ alloy recovered after heating to 2,000 (50) K at 20 (1) GPa in multianvil run with 1 wt% diamond powder. On the XRD pattern *black solid line* represents Rietveld refinement of the experimental data, shown by *red crosses*; elongated *red, fine and bold black strokes* denote position of *fcc-, bcc-Fe,Ni* and Fe_3C phases, respectively. Mössbauer spectrum (*black dots* represent experimental data) was fitted to three Lorentzian line-shape components, corresponding to *fcc-Fe,Ni* (*blue singlet*), *bcc-Fe,Ni* (*grey sextet*) and Fe_3C carbide (*black sextet*)

without Fe_3C formation we carried out another series of LVP quenched experiments with $\text{Fe}_{0.90}\text{Ni}_{0.10-x}\text{C}_x$ ($0.01 \leq x \leq 0.04$, corresponding to approx. $0.2 \leq x \leq 0.9 \text{ wt\%}$) powder mixtures at 0.5–20 GPa and 2,050–2,300 K (see Table 1). Quenched products of LVP runs were analysed by the XRD and Mössbauer spectroscopies, as well as by SEM and TEM. According to the XRD and SEM analyses samples recovered from the LVP runs are homogenous (no evidences of pure iron, nickel or carbon has been detected, as well as no macroscopic phase separation has been observed, see Supplementary figures, Fig. S1), which allows us to make a rough estimation of the solubility of carbon in Fe,Ni based on the composition of the initial mixtures.

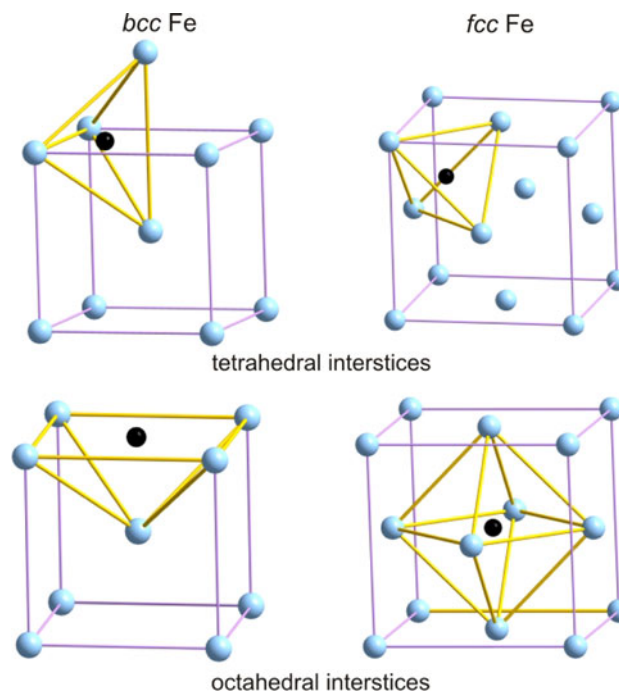


Fig. 6 Location of carbon (*solid spheres*) in octahedral and tetrahedral interstices of *bcc-* and *fcc-*Fe (*opaque spheres*)

All LVP runs performed at pressures from 0.5 to 20 GPa and temperatures from 2,050 (10) K to 2,300 (50) K with $\text{Fe}_{0.90}\text{Ni}_{0.10-x}\text{C}_x$, containing up to 3 at% C as well as runs with 4 at% C at pressures to 9 GPa revealed formation of *bcc*-structured (Fe,Ni)C phase (slightly distorted towards tetragonal symmetry) together with *fcc*-structured (Fe,Ni)C alloy. No Fe_3C carbide crystallization was detected. At the highest carbon contents achieved in this work, 4 at% (or $\sim 0.88 \text{ wt\%}$), tetragonal distortion of *bcc* crystal lattice, *c/a* ratio, was found to be 1.02 (0.01) (Fig. 7) [the calculated value (Eq. 1) is 1.04].

Previous studies of Fe–C martensite (Génin and Flinn 1966; Gielen and Kaplow 1967; Ino et al. 1982; Génin 1987; Dabrowski et al. 1994) suggest that its spectrum consists of as many as three types of Mössbauer components: (1) high intensity ferromagnetic sextet attributed to iron atoms, which do not have carbon atom(s) as the nearest neighbor; (2) low-intensity weak sextet(s) ascribed to the iron atoms in the neighborhood of carbon atom(s); and (3) central peak(s) associated with an antiferromagnetic *fcc*-phase. In general, the number of the type-(ii) sextets varies depending upon the sample purity, processing conditions, test temperature, etc. Génin (1987), using a curve fitting approach, suggested that up to six type-(ii) sextets might be distinguished in the spectrum of the martensite quenched to room temperature. In the present work, however, we obtained a good fit of Mössbauer spectra of martensitic component using model, which

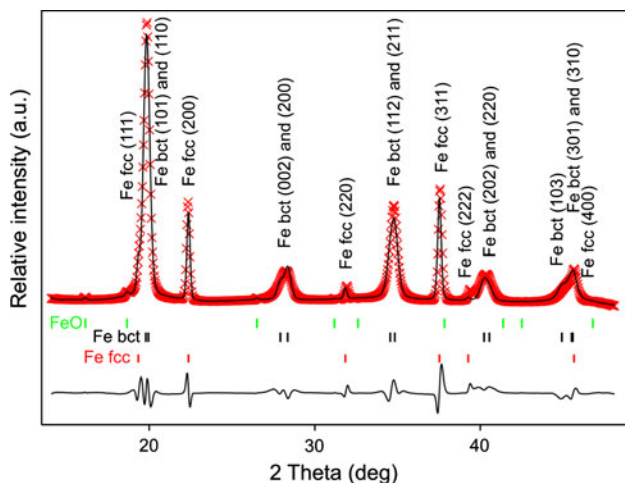


Fig. 7 XRD pattern collected at ambient conditions from $\text{Fe}_{0.90}\text{Ni}_{0.06}\text{C}_{0.04}$ alloy quenched from 2,050 (20) K at 3.0 (0.1) GPa ($\lambda = 0.7002 \text{ \AA}$). Red crosses represent experimental data, the Rietveld refinement is shown by solid black line. Red, black and green elongated strokes denote positions of the reflections of *fcc* (Fe,Ni)C ($a = 3.61000(22) \text{ \AA}$), (*bct*) (Fe,Ni)C ($a = 2.8582(4) \text{ \AA}$, $c = 2.9027(8) \text{ \AA}$) and FeO

contains one sextet ($\text{CS} = 0.03 (0.01) \text{ mm s}^{-1}$, $B = 34.2 (0.3) \text{ T}$) to fit the magnetic *bcc*-structured Fe-bearing component (coloured in light grey in Fig. 8) and one singlet ($\text{CS} = -0.07 (0.01) \text{ mm s}^{-1}$) to fit the antiferromagnetic *fcc*-structured Fe-bearing component (coloured in blue in Fig. 8).

We showed that Fe,Ni alloy can still incorporate 4 at% C at 9 GPa, at 20 GPa presence of this amount of carbon leads to the formation of $(\text{Fe,Ni})_3\text{C}$ carbide (dark grey sextet in Fig. 8b). This agreed with the previously reported compression-induced decrease of carbon solubility in iron

(Wood 1993; Huang et al. 2005; Lord et al. 2009; Nakajima et al. 2009). Note that in all LVP runs performed in the MgO capsule formation of a trace amount of (Fe,Ni)O was also observed. In order to check whether the presence of oxygen affects the phase relations in the Fe–Ni–C system, we repeated some of the LVP runs using NaCl as an internal capsule (to eliminate oxygen from the system) and obtained the same results as in the case of LVP runs performed with MgO capsule. Therefore, we conclude that in the case of LVP runs the effect of oxygen on the phase relations in Fe–Ni–C system is negligible, which allows to compare results of LVP and LH-DAC experiments presented here.

Indirect confirmation of the fact that the observed coexistence of *bcc*- and *fcc*-structured (Fe,Ni)C phases is the result of the martensitic (diffusionless) transformation, induced by rapid cooling, is provided by the TEM analyses. The microstructure of the quenched products was shown to consist of the needle-shaped grains of *bcc*-structured (Fe,Ni)C phase with length of tens of nanometers (Fig. 9a). Such fine structure of the low-carbon iron alloys is well known in metallurgy as the lath martensite, the morphology and crystallography of which has been extensively investigated by optical and TEM, the review can be found in Morito et al. (2006).

In order to confirm that all above-described results are the consequence of the non-equilibrium cooling of Fe–Ni–C system, which promotes martensitic transformation, in several LVP runs the (Fe,Ni)C samples were gradually cooled to 1,000 K at a rate of $1.75^\circ\text{C min}^{-1}$ and then immediately quenched to room temperature. XRD and Mössbauer spectroscopic analyses of the recovered samples revealed the presence of $(\text{Fe,Ni})_3\text{C}$ carbide along with

Fig. 8 Mössbauer spectra collected at ambient conditions from **a** $\text{Fe}_{0.90}\text{Ni}_{0.07}\text{C}_{0.03}$ and **b** $\text{Fe}_{0.90}\text{Ni}_{0.06}\text{C}_{0.04}$ quenched from 2,300 (50) K at 20 GPa (1); $\text{Fe}_{0.90}\text{Ni}_{0.07}\text{C}_{0.03}$ quenched from 2,050 (10) K and 3.0 (0.1) GPa (c) and gradually cooled from 2,050 (10) K to 1,000 (10) K at 3.0 (0.1) GPa (d). Mössbauer components are coloured as following: light grey *bcc*-structured (Fe,Ni)C phase, light blue *fcc*-structure (Fe,Ni)C phase, and dark grey Fe_3C carbide

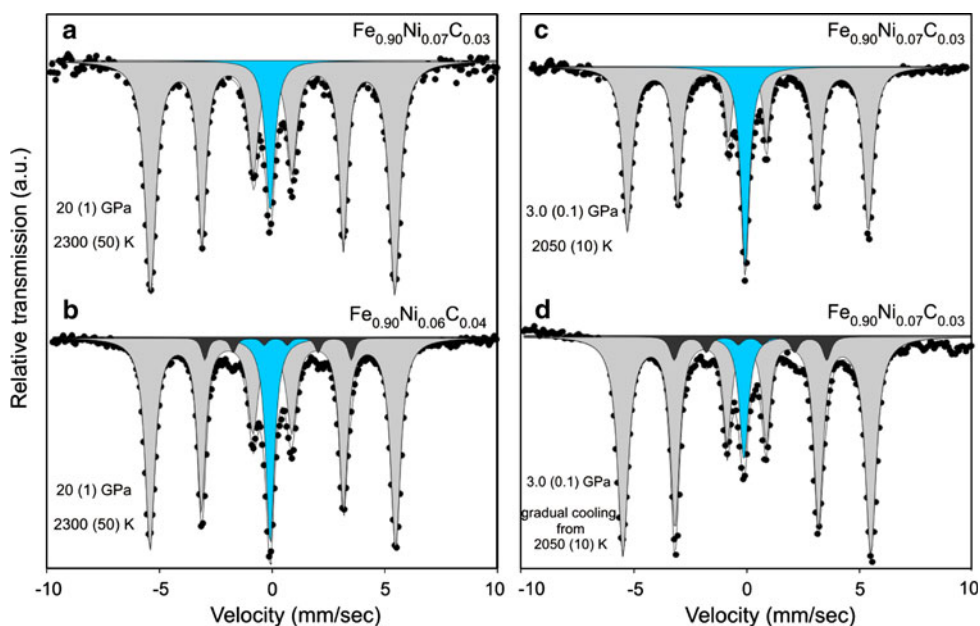
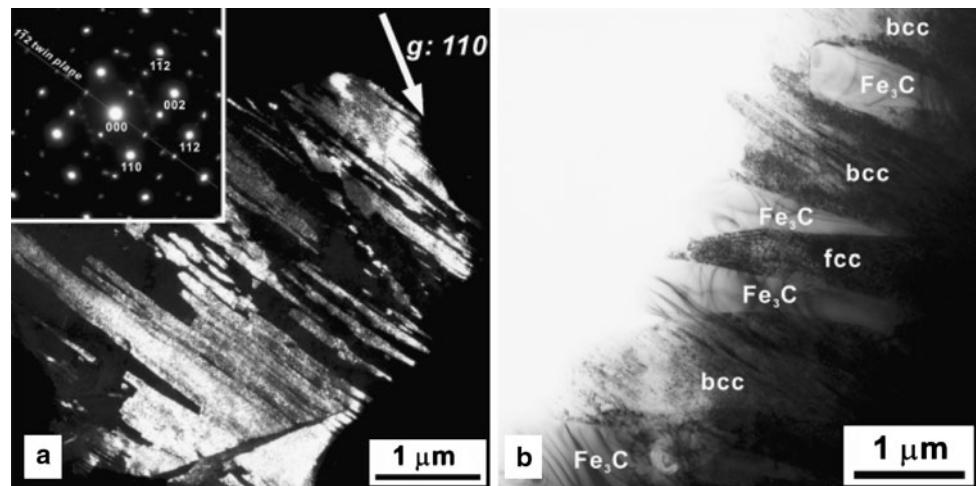


Fig. 9 TEM images obtained from **a** $\text{Fe}_{0.90}\text{Ni}_{0.08}\text{C}_{0.02}$ recovered after heating to 2,100 (50) K at 9 (1) GPa and **b** $\text{Fe}_{0.90}\text{Ni}_{0.07}\text{C}_{0.03}$ gradually cooled to from 2,050 (10) K to 1,000 (10) K at 2.0 (0.1) GPa. **a** Dark-field image with $g = 110_{bcc}$. The selected area electron diffraction (*inset*) indicates a $\{112\}$ twin (**b**) bright-field image of the *fcc* phase (centre, between two Fe_3C phases) coexisting with the Fe_3C phase and the *bcc* phase



bcc- and *fcc*-structured (Fe,Ni)C alloys (Fig. 8d). TEM analyses of one of the quenched experiment, performed with $\text{Fe}_{0.90}\text{Ni}_{0.07}\text{C}_{0.03}$ stoichiometric mixture at 2.0(1) GPa (Fig. 9b), confirms the presence of *bcc*- $\text{Fe}_{0.91}\text{Ni}_{0.09}$ and *fcc*- $\text{Fe}_{0.83}\text{Ni}_{0.17}$ alloys together with $(\text{Fe}_{0.97},\text{Ni}_{0.03})_3\text{C}$ carbide (the chemical composition was estimated by means of TEM–EDXS).

Iron carbides in Earth's core?

Estimates of the amount of carbon in Earth's core vary from as low as 0.2 to 0.4 wt% (McDonough and Sun 1995; Dasgupta and Walker 2008), which makes carbon a plausible candidate for the light component in the core, or at least a part of it. As mentioned earlier, the pressure effect on the eutectic composition in Fe– Fe_3C has not been conclusively constrained. According to Wood (1993), Huang et al. (2005), Lord et al. (2009) and Nakajima et al. (2009) the Fe– Fe_3C eutectic moves to nearly pure iron at high pressure, while Fei et al. (2007) reported opposite behaviour of Fe–C system upon compression. Our experimental results clearly suggest the decrease of carbon solubility in Fe,Ni upon compression. The interplay between the amount of carbon available in Earth's core and the Fe–Ni–C eutectic composition at the relevant pressures and temperatures would provide a hint to what phases might crystallize in the Earth's inner core, as well as would constrain the concentration of carbon in the outer core. If the eutectic composition of Fe–Ni–C system moves towards pure Fe,Ni at the core conditions than the inner core would crystallize, at least partially, as a carbide phase depleting the outer core in carbon. According to Lord et al. (2009) and Nakajima et al. (2009) Fe_7C_3 rather than Fe_3C seems to be the most plausible candidate in this scenario. However, a reverse situation cannot be excluded—if the core is significantly depleted in carbon, then the entire carbon budget would be stored in the outer core while the

inner core would crystallize as a metallic Fe,Ni phase. In order to provide a decisive constraint on the partitioning of carbon between inner and outer parts of Earth's core the eutectic composition of Fe,Ni–C system at the relevant pressures and temperatures need to be constrained. The effect of other possible light components (Si, O, S, etc.) also has to be taken into account.

Conclusions

We carried out a systematic comparative study of $\text{Fe}_{1-x}\text{Ni}_x$ ($0.1 \leq x \leq 0.22$) alloys at pressures to 45 GPa in temperature range 296–2,600 K using LH-DAC and LVP techniques. The laser heating in DAC even at relatively low temperatures, 1,700–1,800 K, can induce diffusion of carbon from the diamond anvils, which can contaminate the sample. Therefore, the experimental results obtained in LH-DAC experiments should be interpreted with great caution. Laser-heating-induced diffusion of carbon can be considered as a plausible reason for systematic lowering of the melting curve of iron obtained in LH-DAC experiments with respect to the theoretical predictions and shock-wave measurements.

Our LVP experiments with $\text{Fe}_{0.90}\text{Ni}_{0.10-x}\text{C}_x$ at pressures 0.5–20.0(5) GPa and temperatures 2,050 (10)–2,300 (50) K suggest that *fcc*-structured Fe,Ni alloy can incorporate as much as 0.9 wt% carbon at pressures to 9 GPa; and via diffusionless martensitic transformation this alloy can be quenched to ambient conditions without formation of Fe_3C carbide. Our results suggest the decrease of carbon solubility in Fe,Ni alloy with increase of pressure, which coincides with previously reported shift of the eutectic composition towards carbon-depleted part of the Fe–C phase diagram (Wood 1993; Huang et al. 2005; Lord et al. 2009; Nakajima et al. 2009), which most probably would result in the crystallization of a certain amount of Fe_7C_3

carbide in Earth's inner core (Lord et al. 2009; Nakajima et al. 2009).

Acknowledgments The project was partly supported by funds from the German Science Foundation (DFG) Priority Programme SPP1236 under project Mc 3/16-1 and the Eurocores EuroMinSci Programme. We thank Daniel J. Frost (Bayerisches Geoinstitut) for help with multianvil experiments as well as Hubert Schulze and Uwe Dittmann (Bayerisches Geoinstitut) for preparation of the quenched samples for further analyses.

References

- Akimoto S (1987) High-pressure research in geophysics: past, present, and future, in high-pressure research in mineral physics. In: Manghnani MH, Syono Y (eds) Terra Scientific Publishing Company, Tokyo, pp 1–13
- Alfè D (2009) Temperature of the inner-core boundary of the Earth: melting of iron at high pressure from first-principles coexistence simulations. *Phys Rev B (Rapid)* 79:060101(R)
- Allègre CJ, Poirier J-P, Humler E, Hofmann AW (1995) The chemical composition of the Earth. *Earth Planet Sci Lett* 134:515–526
- Badding JV, Mao H-K, Hemley RJ (1991) High-pressure chemistry of hydrogen in metals: in-situ study of iron-hydrate. *Science* 253:421–424
- Birch F (1952) Elasticity and constitution of the Earth's interior. *J Geophys Res* 57:227–286
- Boehler R (1986) The phase diagram of iron to 430 kbar. *Geophys Res Lett* 13:1153–1156
- Boehler R (1993) Temperatures in the Earth's core from melting-point measurements of iron at high static pressures. *Nature* 363:534–536
- Brown JM (2000) The NaCl pressure standard. *J Appl Phys* 86: 5801–5808
- Brown JM, McQueen RG (1986) Phase transitions, Grüneisen parameter, and elasticity for shocked iron between 77 GPa and 400 GPa. *J Geophys Res* 91:7485–7494
- Cliff G, Lorimer GW (1975) The qualitative analysis of thin specimens. *J Microsc* 103:203–207
- Cohen RE, Mukherjee S (2004) Non-collinear magnetism in iron at high pressures. *Phys Earth Planet Int* 143–144:445–453
- Dabrowski L, Suwalski J, Sidzhimov B, Christov V (1994) Investigations of ordering dynamics in carbon martensite. *Acta Metall Mater* 42(7):2375–2380
- Dasgupta R, Walker D (2008) Carbon in the core melts in a shallow magma ocean environment and distribution of carbon between the Earth's core and the mantle. *Geochim Cosmochim Acta* 72:4627–4641
- Dewaele A, Loubeyre P, Occelli F et al (2006) Quasihydrostatic equation of state of iron above 2 Mbar. *Phys Rev Lett* 97:215504–215507
- Dubrovinsky LS, Saxena SK, Lazor P (1998) High-pressure and high-temperature X-ray diffraction study of iron and corundum to 68 GPa using an internally heated diamond anvil cell. *Phys Chem Miner* 25:434–441
- Dubrovinsky LS, Dubrovinskaia NA, Abrikosov IA et al (2001) Pressure induced invar effect in Fe,Ni alloys. *Phys Rev Lett* 86:4851–4854
- Dubrovinsky LS, Dubrovinskaia NA, Narygina O et al (2007) Body-centered cubic iron–nickel alloy in Earth's core. *Science* 316:1880–1883
- Fei Y, Mao H-K (1994) In situ determination of the Ni–As phase of FeO at high pressure and temperature. *Science* 266:1678–1680
- Fei Y, Preitt CT, Mao H-K, Bretka CM (1995) Structure and density of FeS at high pressure and high temperature and the internal structure of Mars. *Science* 268:1892–1894
- Fei Y, Li J, Bertka CM, Preitt CT (2000) Structure type and bulk modulus of Fe₃S a new iron–sulfur compound. *Am Mineral* 85:1830–1833
- Fei Y, Wang Y, Deng L (2007) Melting relations in Fe–C–S system at high pressure implications for the chemistry of the cores of terrestrial planets. *Lunar and Planetary Science conference XXXVIII*, abstract 1231
- Fialin M, Catillon G, Andraut D (2009) Disproportionation of Fe²⁺ in Al-free silicate perovskite in the laser heated diamond anvil cell as recorded by electron probe microanalysis of oxygen. *Phys Chem Miner* 36:183–191
- Frost DJ, Langenhorst F, van Aken PA (2001) Fe–Mg partitioning between ringwoodite and magnesiowüstite and the effect of pressure, temperature and oxygen fugacity. *Phys Chem Miner* 28:455–470
- Funamori N, Yagi T, Uchida T (1996) High-pressure and high-temperature in-situ X-ray diffraction study of iron to above 68 GPa using MA8-type apparatus. *Geophys Res Lett* 23:953–956
- Génin J-M (1987) The clustering and coarsening of carbon multiplets during the aging of martensite from Mössbauer spectroscopy: the pre-precipitation stage of epsilon carbide. *Metall Mater Trans A* 18:1371–1388
- Génin J-M, Flinn PA (1966) Mössbauer effect evidence for the clustering of carbon atoms in iron–carbon martensite during aging at room temperature. *Phys Lett* 22:392–393
- Gielen PM, Kaplow R (1967) Mössbauer effect in iron–carbon and iron–nitrogen alloys. *Acta Metall* 15:49–63
- Greenwood NN, Gibb TC (1971) Mössbauer spectroscopy. Chapman and Hall, London, pp 314–315 and the references therein
- Gulyaev AP (1977) *Metallovedenie, metallurgy*, Moscow
- Hammersley AP (1998) FIT2D V9.129 reference manual V3.1 ESRF internal report ESRF98HA01T. http://www.esrf.eu/computing/scientific/FIT2D/FIT2D_REF/fit2d_r.html
- Heinz DL, Sweeney JS, Miller P (1991) A laser-heating system that stabilizes and controls the temperature—diamond anvil cell applications. *Rev Sci Instrum* 62:1568–1575
- HStC O'Neill, Palme H (1998) Composition of the silicate Earth: implications for accretion and core formation. In: Jackson I (ed) *The Earth's mantle*. Cambridge University Press, Cambridge, pp 3–12
- Huang E, Bassett W, Weathers MS (1988) Phase relationships in Fe,Ni alloys at high pressures and temperatures. *J Geophys Res* 93:7741–7746
- Huang E, Bassett W, Weathers MS (1992) Phase diagram and elastic properties of Fe 30% Ni alloy by synchrotron radiation. *J Geophys Res* 97:4497–4502
- Huang L, Skorodumova NV, Belonoshko AB et al (2005) Carbon in iron phases under high pressure. *Geophys Res Lett* 32:L21314
- Ino H, Ito T, Nasu S, Gonser U (1982) A study of interstitial atom configuration in fresh and aged iron–carbon martensite by Mossbauer spectroscopy. *Acta Metall* 30:9–20
- Jiang DE, Carter EA (2003) Carbon dissolution and diffusion in ferrite and austenite from first principles. *Phys Rev B* 67:214103–214111
- Kakeshita T, Shimizu K, Akahama Y et al (1988) Effect of hydrostatic pressure on martensitic transformations in Fe,Ni and Fe,Ni–C alloys. *Trans Jpn Inst Met* 29:109–115
- Knittel E, Williams Q (1995) Static compression of ε-FeSi and evolution of reduced silicon as a deep Earth constituent. *Geophys Res Lett* 22:445–448
- Komabayashi T, Fei Y, Meng Y, Prakapenka V (2009) In-situ X-ray diffraction measurements of the γ–ε transition boundary of iron

- in an internally-heated diamond anvil cell. *Earth Planet Sci Lett* 282:252–257
- Kubo A, Akaogi M (2000) Post-garnet transitions in the system $\text{Mg}_4\text{Si}_4\text{O}_{12}$ – $\text{Mg}_3\text{Al}_2\text{Si}_3\text{O}_{12}$ up to 28 GPa: phase relations of garnet, ilmenite, and perovskite. *Phys Earth Planet Inter* 125:105–112
- Kubo A, Ito E, Katsura T, Shinmei T, Yamada H, Nishikawa O, Song M, Funakoshi K (2003) In situ X-ray observation of iron using Kawai-type apparatus equipped with sintered diamond: absence of β phase up to 44 GPa and 2,100 K. *Geophys Res Lett* 30:1126–1130
- Kurdjumov G, Kaminsky E (1928) X-ray studies of the structure of quenched carbon steel. *Nature* 122:475–476
- Kurdjumov G, Kaminsky E (1929) Eine röntgenographische Untersuchung der Struktur des gehärteten. Kohlenstoffstahls *Z Phys* 53:696–707
- Lai A, Bernard S, Chiarotti GL et al (2000) Physics of iron at Earth's core conditions. *Science* 287:1027–1030
- Larson AC, Von Dreele RB (2004) General structure analysis system (GSAS). Los Alamos National Laboratory Report LAUR 86, p 748
- Lin J-F, Heinz DL, Campbell AJ et al (2002) Iron–nickel alloy in the Earth's core. *Geophys Res Lett* 29:109–111
- Liu J, Dubrovinsky LS, Boffa Ballaran T, Crichton W (2007) Equation of state and thermal expansivity of LiF and NaF. *High Press Res* 27:483–489
- Lord OT, Walter MJ, Dasgupta R et al (2009) Melting in the Fe–C system to 70 GPa. *Earth Planet Sci Lett* 284:157–167
- Manghnani MH, Syono Y (1987) High pressure research in mineral physics. Terra Scientific Publishing Company, Tokyo
- Mao H-K, Xu J, Bell PM (1986) Calibration of the ruby pressure gage to 800 kbar under quasi-hydrostatic conditions. *J Geophys Res* 91:4673–4676
- Mao H-K, Bell PM, Hadidiacos C (1987) Experimental phase relations of iron to 360 kbar, 1,400 C, determined in and internally heated diamond-anvil apparatus. In: Manghnani MH, Syono Y (eds) High pressure research in mineral physics. Terra Scientific Publishing Company, Tokyo, pp 135–138
- Mao W, Campbell AJ, Heinz DL, Shen G (2006) Phase relations of Fe,Ni alloys at high pressure and temperature. *Phys Earth Planet Inter* 155:146–151
- Martens A (1878a) Ueber die mikroskopische Untersuchung des Eisens. *Z Vereines Deutscher Ingenieure* 22:11–18
- Martens A (1878b) Zur Mikrostruktur des Spiegeleisens—Die Erscheinungen auf den Bruchflächen. *Z Vereines Deutscher Ingenieure* 22:205–214
- Martens A (1878c) Zur Mikrostruktur des Spiegeleisens—Die Erscheinungen auf den Schlißflächen. *Z Vereines Deutscher Ingenieure* 22:481–488
- Mazur J (1950) Lattice parameters of martensite and of austenite. *Nature* 166:828
- McCammon CA, Rubie DC, Ross CR II, Siefert F, HStC O'Neill (1992) Mössbauer spectra of $^{57}\text{Fe}_{0.05}\text{Mg}_{0.95}\text{SiO}_3$ perovskite at 80 and 298 K. *Am Mineral* 77:894–897
- McDonough WF, Sun S-S (1995) The composition of the Earth. *Chem Geol* 120:223–253
- Morito S, Huang X, Furuhashi T et al (2006) The morphology and crystallography of lath martensite in alloy steels. *Acta Mater* 54:5323–5331
- Murakami M, Hirose K, Sata N, Ohishi Y (2005) Post-perovskite phase transition and mineral chemistry in the pyrolytic lowermost mantle. *Geophys Res Lett* 32:L033004.1–L033004.4
- Nakajima T, Takahashi E, Suzuki T, Funakoshi KI (2009) “Carbon in the core” revisited. *Phys Earth Planet Inter* 174:202–211
- Ohta K, Onoda S, Hirose K et al (2008) The electrical conductivity of post-perovskite in Earth's D'' layer. *Science* 320:89–91
- Patel JR, Cohen M (1953) Criterion for the action of applied stress in the martensitic transformation. *Acta Metall* 1:531–538
- Poirier J-P (1994) Light elements in the Earth's outer core: a critical review. *Phys Earth Planet Inter* 85:319–337
- Prakapenka VB, Shen G, Dubrovinsky LS (2003/2004) Carbon transport in diamond anvil cells. *High Temp High Press* 35/36:237–249
- Ringwood AE (1979) Origin of the Earth and Moon. Springer, Berlin
- Roberts CS (1953) Effect of carbon on the volume fractions and lattice parameters of retained austenite and martensite. *Trans Am Inst Metall Eng* 197:203–204
- Rouquette J, Dolejš D, Kantor IYu et al (2008) Iron–carbon interactions at high temperatures and pressures. *Appl Phys Lett* 92:121912.1–121912.3
- Sanloup C, Guyot F, Gillet P et al (2000) Density measurements of liquid Fe–S alloys at high-pressure. *Geophys Res Lett* 27:811–814
- Schen G, Mao H-K, Hemley RJ et al (1998) Melting and crystal structure of iron at high pressures and temperatures. *Geophys Res Lett* 25:373–376
- Scott HP, Williams Q, Knittle E (2001) Stability and equation of state of Fe_3C to 73 GPa: implications for carbon in the Earth's core. *Geophys Res Lett* 28:1875–1878
- Shackelford J (2001) CRC materials science and engineering handbook. CRC Press, Boca Raton
- Shallcross S, Kissavos AE, Sharma S, Meded V (2006) Noncollinear order in the γ -Fe system: generalized Heisenberg approach. *Phys Rev B* 73:104443–104448
- Stevens W, Haynes AG (1956) The temperature of forming martensite and bainite in low-alloy steels. *J Iron Steel Inst* 183:349–359
- Stixrude L, Cohen RE, Singh DJ (1994) Iron at high pressure: linearized-augmented-plane-wave computations in the generalized-gradient approximation. *Phys Rev B* 50:6442–6445
- Troiano A, Greninger A (1946) The martensite transformation. *Metal Prog* 50:303–307
- Vocadlo L, Alfè D, Brodholt J et al (2000) Ab-initio free energy calculations on the polymorphs of iron at core conditions. *Phys Earth Planet Inter* 117:123–137
- Williams Q, Jeanloz R, Bass J et al (1987) The melting curve of iron to 250 gigapascals: a constraint on the temperature at the Earth's center. *Science* 236:181–182
- Wood BJ (1993) Carbon in the core. *Earth Planet Sci Lett* 117:593–607
- Xiao L, Fan Z, Jinxiu Z (1995) Lattice-parameter variation with carbon content of martensite. I. X-ray-diffraction experimental study. *Phys Rev B* 52:9970–9978
- Xie ZL, Sundqvist B, Hiinninen H et al (1993) Isothermal martensitic transformation under hydrostatic pressure in an Fe,Ni–C alloy at low temperatures. *Acta Metall Mater* 41:2283–2290
- Yoo CS, Holmes NC, Ross M et al (1993) Shock temperatures and melting of iron at Earth core conditions. *Phys Rev Lett* 70:3931–3934